Results in Physics 19 (2020) 103408

Contents lists available at ScienceDirect

Results in Physics

journal homepage: www.elsevier.com/locate/rinp

First-principles calculations into $LiAl(NH_2)_4$ and its derivative hydrides for potential sodium storage

Yingying Ren [a], Xiaohan Ren [a], Rajeev Ahuja [b,c], Zhao Qian [a,*]

[a] Key Laboratory of Liquid-Solid Structural Evolution and Processing of Materials (Ministry of Education) & Institute of Thermal Science and Technology, Shandong University, 250061 Jinan, China
[b] Condensed Matter Theory, Department of Physics, Ångström Laboratory, Uppsala University, 75120 Uppsala, Sweden
[c] Applied Materials Physics, Department of Materials Science and Engineering, Royal Institute of Technology (KTH), 10044 Stockholm, Sweden

ARTICLE INFO

Keywords:
First-principles physics
Atomic-scale design
Light metal based complex hydrides
Sodium-ion battery
Density Functional Theory
Electronic structures

ABSTRACT

In this work, we have employed the first-principles quantum physics method to investigate the light-metal based $LiAl(NH_2)_4$ and its modified compounds as conversion electrode materials for sodium-ion batteries on the basis of state-of-the-art Density Functional Theory. The pure $LiAl(NH_2)_4$ possesses an average voltage of 0.294 V (versus Na^+/Na^0) and a theoretical specific capacity of 1093.77 mA h g^{-1} for sodium storage. Among the modified materials, the $Li_4AlB_3(N_4H_8)_4$ has the most excellent electrochemical properties with a theoretical specific capacity of 1249.57 mA h g^{-1} and a low average voltage of 0.087 V (versus Na^+/Na^0) for potential anode applications. The diffusion behavior of Na-ion is also improved in $Li_4AlB_3(N_4H_8)_4$ whether at 300 K or at 400 K, which indicates the prospective rate capability. The diffusion coefficient of Na-ion is obviously increased to 3.667×10^{-9} m^2 s^{-1} (in modified material) from 1.500×10^{-9} m^2 s^{-1} (in pristine material) at 400 K. The diffusion of Na-ion is calculated to be very fast in $Li_4AlB_3(N_4H_8)_4$ with a kinetic barrier of 0.31 eV. This work will provide impetus to the quantum design and experimental development of complex hydride materials for metal-ion battery applications.

Introduction

Due to environmental pollution and the finite reserve of fossil fuels, the world's demand for green and clean energy is becoming more and more urgent. With the rapid development of society, the clean electric energy accounts for an increasing proportion in human energy use. In the current era, the lithium battery is playing an important role in electricity storage. However, due to the uneven distribution and relative shortage of lithium resources, the large-scale industry urgently seeks for lower-cost and more abundant resources for energy storage [1–3]. The sodium element which is in the same main group with lithium owns some similar physicochemical properties [4]. Geological surveys show that the abundance of sodium (2.75%) is significantly higher than that of lithium (0.002%) in the Earth crust and the sodium is widely distributed and readily available in the world [5]. Therefore, sodium-ion batteries (SIBs) are usually regarded as one of the most outstanding candidates especially for large-scale industrial system applications [6,7]. While, since the sodium-ion has a larger radius than lithium, most of the electrode materials for lithium batteries are not suitable for sodium storage such as the commercial graphite anode materials [8,9]. Oumellal et al. propounded a new notion of using metal hydride as the negative electrode of battery, which provided great inspiration to get beyond the delamination/intercalation mechanism [10,11]. Their ability to undergo conversion reactions with lithium to function as capacitive anodes or to transport Li ions to perform as competent super-ionic conductors has been demonstrated [12–18]. While at present, the exploration of metal hydride materials' utilization in sodium ion batteries (SIBs) is very scarce. Attentions have been paid to electrode materials with appropriate redox potentials and high specific capacities with excellent electrochemical properties [19–21]. According to previous reports, metal hydrides showed the lowest polarization for conversion reaction materials. Compared with sulfides, phosphides, oxides, nitrides, and fluorides, using metal hydrides as the negative electrode of sodium-ion battery will have far-reaching significance to the promotion of sodium-ion battery and utilization of clean energy [22,23]. In 2002, Chen et al. proposed that the MNH (metal nitrogen hydrides) could release and absorb hydrogen reversibly in large quantity, which aroused people's attention to the research of metal nitrogen hydrides for hydrogen

* Corresponding author.
E-mail address: qianzhao@sdu.edu.cn (Z. Qian).

https://doi.org/10.1016/j.rinp.2020.103408
Received 14 July 2020; Received in revised form 26 August 2020; Accepted 10 September 2020
Available online 15 September 2020

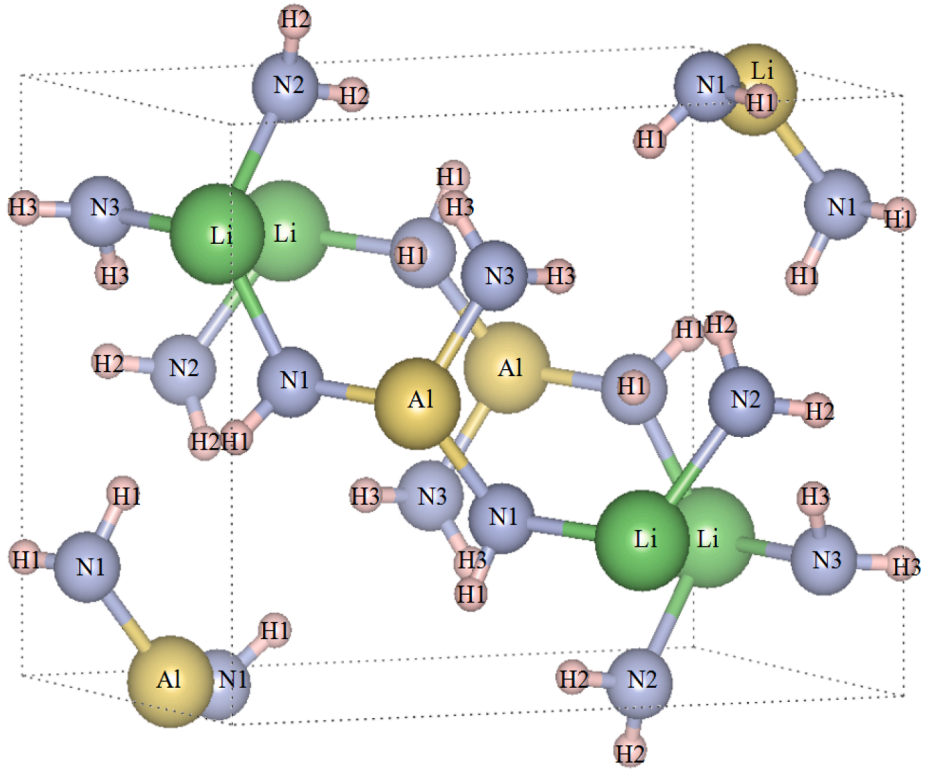

Fig. 1. The complex structure of $LiAl(NH_2)_4$ (56 atoms each unit cell) after structural optimizations. The green, gold, blue, and pink balls represent Li, Al, N, and H atoms, respectively. The atomic sites are distinguished by Arabic numbers. (For interpretation of the references to color in this figure legend, the reader is referred to the web version of this article.)

storage materials [24]. In the application of thermal-chemical hydrogen storage, people pay more attention to whether the material has excellent reversible property of hydrogen absorption and release. While for the electrochemical energy storage applications, the physical understanding of electrode reaction is the key to utilizing metal hydrides [25–28].

One of the powerful tools to understand many properties of materials is first-principles calculations [29–31]. The first-principles method is also of significance in dissecting the electrochemical performance of electrode materials and designing high performance sodium-ion battery materials [32–34]. Theoretical screening of electrode materials can lay important foundation for the selection of promising material(s) for battery applications, avoid a large number of blind experiments and help the development of excellent electrode materials more efficiently [35–42]. In this work, our investigation aims at exploring the potential properties of $LiAl(NH_2)_4$ and its derivative materials for sodium-ion battery applications. The structural, electronic, electrochemical and diffusion-related kinetic properties are taken into consideration. We have chosen the two elements K (in the same main group as Li) and B (in the same main group as Al) for modifying the pristine compound. The different concentrations of B and K are also considered for modification to achieve better electrochemical properties and the diffusion kinetics of sodium-ions in these systems are also investigated. This quantum-mechanical study is proposed to help to understand the energy storage properties of the materials [43–45]. Furthermore, our findings have important implications for advancing the atomic-scale understanding of MNH (metal nitrogen hydrides) as potential conversion electrode materials in sodium-ion batteries (SIBs) and make important contribution and guide to the experimental development of the related materials for energy storage.

Methods

All the computational sections were carried out by Density Functional Theory (DFT) method as implemented in Vienna Ab initio Simulation Package [46–48]. The inner electrons were represented by projector augmented wave (PAW) pseudopotentials [49,50]. The exchange correlation energy was treated by the Perdew-Burke-Ernzerhof (PBE) functional within the generalized gradient approximation (GGA) [51,52]. The crystal structures were optimized by the conjugate gradient algorithm. The Brillouin zone was sampled by $5 \times 5 \times 7$ k-points using Monkhorst-Pack scheme in structural relaxations and the k-point of $1 \times 1 \times 1$ was employed in time-consuming ab initio molecular dynamics (AIMD) calculations. We adopted the plane wave basis set with an energy cutoff of 520 eV. The force and energy convergence thresholds for structural optimizations were set to 0.02 eV/Å and 10^{-4} eV, respectively. The calculation cell was enlarged to a supercell of $2 \times 2 \times 1$ during the computations of mean squared displacement and diffusion coefficient. The Bader charge analysis was used to unveil the charge transfer inside the electrode materials.

During the investigations of Na-ion diffusion behavior in $Li_4Al_4(N_4H_8)_4$ and $Li_4AlB_3(N_4H_8)_4$, some images were constructed using the linear interpolation method in CI-NEB [53,54]. The transition state in minimum energy pathway (MEP) was computed to obtain the diffusion barrier. The optimization thresholds were 10^{-4} eV and 0.05 eV/Å for electronic and ionic relaxation, respectively. The spin-polarized calculations were performed throughout the work.

Results and discussion

The low-temperature phase of $LiAl(NH_2)_4$ is illustrated in Fig. 1. The geometrically optimized lattice parameters of the structure are: $a = 9.499$ Å, $b = 7.373$ Å, $c = 7.476$ Å and $\alpha = \gamma = 90°$, $\beta = 90.11°$ with a monoclinic structure (space group of P21/n). There are 4 Al atoms, 4 Li atoms, 16 N atoms and 32 H atoms ($Li_4Al_4(N_4H_8)_4$) in each unit cell. The calculated lattice parameters are consistent with the results obtained in experiments or other related computational works [55–57]. In the

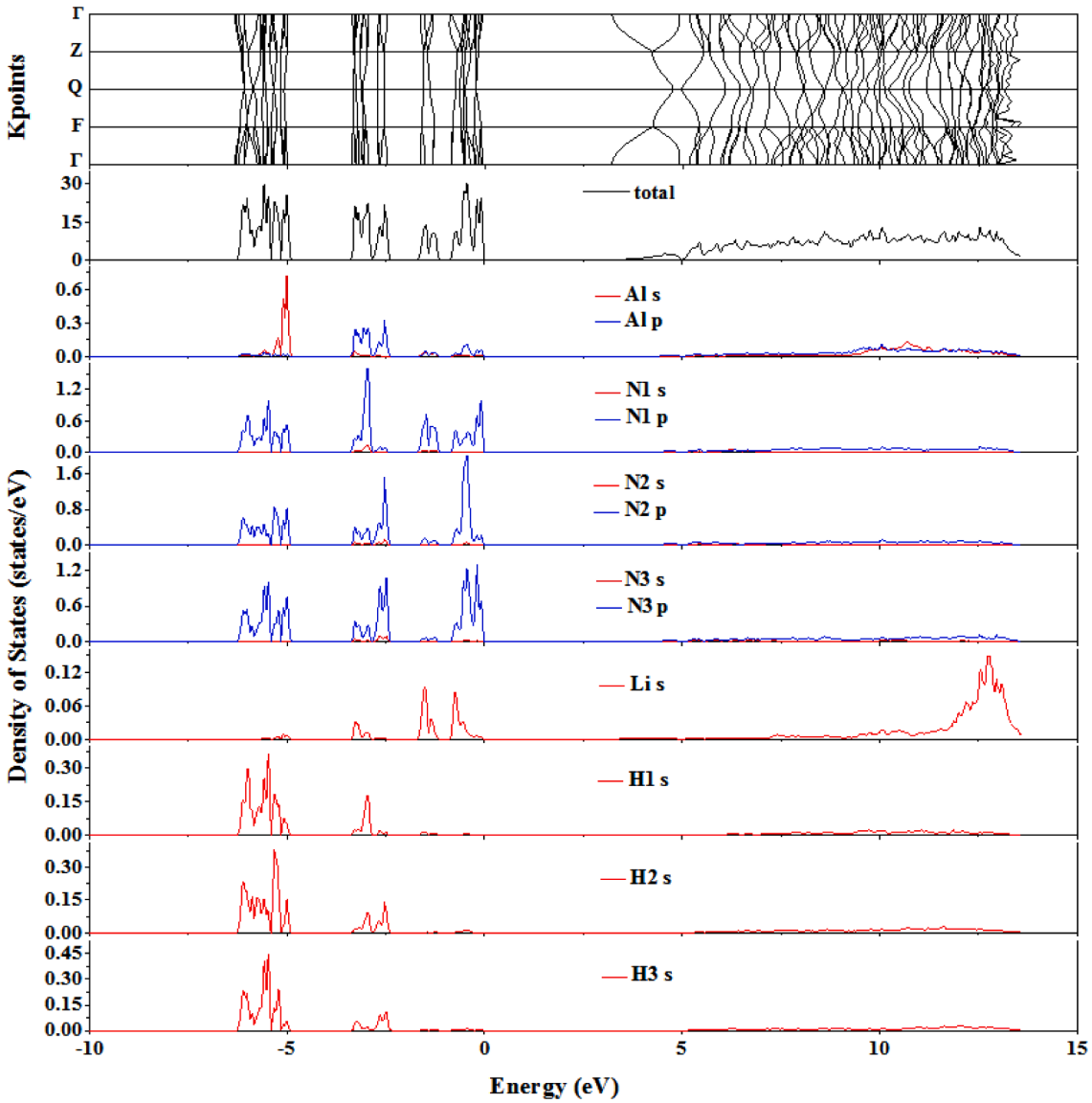

Fig. 2. The electronic band structure, the total and partial density of states (DOS) for pristine $LiAl(NH_2)_4$. The s and p states are represented by red and blue colors respectively. The Fermi energy level is set at zero. (For interpretation of the references to color in this figure legend, the reader is referred to the web version of this article.)

structure, the 4 Al atoms are equivalent in site occupancy and 4 Li atoms as well. While, the 32 H atoms are classified into three different kinds of sites that are marked as H1, H2 and H3. Each unit cell has three different N sites that are designated as N1, N2 and N3 site respectively. The pristine $Li_4Al_4(N_4H_8)_4$ lattice has an ordered structure to potentially accommodate sodium-ions and facilitate the sodium-ion's diffusion through atomic gaps or interstitial spaces.

It is important to analyze the electronic density of states when exploring the chemical bonding in materials. As shown in Fig. 2, the total and partial DOS of the pristine $LiAl(NH_2)_4$ solid are given. The total DOS of $LiAl(NH_2)_4$ consists of three parts: the part below −2.417 eV corresponds to the lower energy region of valence band; the part from −1.662 eV to 0 eV corresponds to the higher valence band; and the part above 3.302 eV corresponds to the conduction band. From the partial DOS, there emerges distinct energy overlapping regions of N1 p-states and H1 s-states. Analogical cases are applied to N2 p-states and H2 s-states as well as N3 p-states and H3 s-states. This sp hybridization between N and H in valence band results in the strong bonding between N1 and H1, N2 and H2, N3 and H3 respectively. The bonding electrons are mainly those whose energy is between −1.662 eV and Fermi level.

In view of the strategy that modification is a valid approach to improving the electrochemical properties of materials, we have used different concentrations of B or K elements (as mentioned in the introduction) to modify the pristine material in this study. Their designation can be expressed as $Li_4Al_3B(N_4H_8)_4$, $Li_4Al_2B_2(N_4H_8)_4$, $Li_4AlB_3(N_4H_8)_4$, $Li_3KAl_4(N_4H_8)_4$, $Li_2K_2Al_4(N_4H_8)_4$, and $LiK_3Al_4(N_4H_8)_4$ respectively. We have substituted Al atoms or Li atoms in the 56-atom unit cell by B atoms or K atoms, which correspond to the modifying concentration of 1.79 at. %, 3.57 at.% and 5.36 at.%. In order to find the most reasonable modified structure, we have completely relaxed the crystal structures and determined the most stable site by referring to the value of formation energy after geometry optimizations. The formation energy can be calculated as follows:

$$E_f = E_T(M) + \mu_h - -\mu_m - E_T(P) \quad (1)$$

where $E_T(M)$ and $E_T(P)$ represent the total energy of the modified and pristine structure respectively, μ_h and μ_m mean the atomic potential of the host and modifying atoms [58]. When one B or K atom substitutes a single Al or Li atom at the concentration of 1.79 at.%, the calculated

Table 1
The calculated formation energies (eV/f.u.) for B- or K-modified $LiAl(NH_2)_4$.

Site	Element	
	B	K
Al site	−2.740	9.142
Li site	−1.003	1.930

formation energies are given in Table 1. It is clear that when the B element is utilized, the formation energy is lower when occupying the Al position. This indicates that the Al site is more thermodynamically favorable for the modification by the B atom. The formation energy is lower when the K atom occupies the Li atom instead of the Al site. We can conclude that the Li site is more thermodynamically favorable for the modification by K.

The charging and discharging conversion reactions of various $LiAl(NH_2)_4$ derivative electrode materials are then investigated, described by the following half-cell reactions versus $Na^+/Na°$ in (2)–(8). The volume changes of various systems before and after conversion reactions are illustrated in Fig. 3(a). Most of the modifications increase the volume change. While, compared with the pristine system, the band gaps of all the modified systems are decreased in Fig. 3(b). The average voltage (versus $Na^+/Na°$) of various derivative materials for sodium-storage electrodes is obtained by the formula (9) [59] where ΔG is the Gibbs free energy variation of the reactions from (2)–(8) respectively and F is the Faraday constant. All the average voltage values versus Na^+/Na^0 are below 0.6 V, i.e. 0.294 V for $Li_4Al_4(N_4H_8)_4$, 0.225 V for $Li_4Al_3B(N_4H_8)_4$, 0.156 V for $Li_4Al_2B_2(N_4H_8)_4$, 0.087 V for $Li_4AlB_3(N_4H_8)_4$, 0.299 V for $Li_3KAl_4(N_4H_8)_4$, 0.578 V for $Li_2K_2Al_4(N_4H_8)_4$ and 0.335 V for $LiK_3Al_4(N_4H_8)_4$ respectively as described in Fig. 3(c). In addition, the theoretical specific capacities of various electrode materials can be calculated according to the formula (10), in which M stands for the molar mass of the anode material and n means the quantity of electrons involved in the electrode reactions. $Li_4AlB_3(N_4H_8)_4$ has the highest specific capacity and the lowest average voltage as shown in Fig. 3(d).

$$Li_4Al_4(N_4H_8)_4 + 16Na^+ + 16e^- = 8NaH + 4AlN + 4LiNH_2 + 8NaNH_2 \quad (2)$$

$$Li_4Al_3B(N_4H_8)_4 + 16Na^+ + 16e^- = 8NaH + 3AlN + BN + 4LiNH_2 + 8NaNH_2 \quad (3)$$

$$Li_4Al_2B_2(N_4H_8)_4 + 16Na^+ + 16e^- = 8NaH + 2AlN + 2BN + 4LiNH_2 + 8NaNH_2 \quad (4)$$

$$Li_4AlB_3(N_4H_8)_4 + 16Na^+ + 16e^- = 8NaH + AlN + 3BN + 4LiNH_2 + 8NaNH_2 \quad (5)$$

$$Li_3KAl_4(N_4H_8)_4 + 16Na^+ + 16e^- = 8NaH + 4AlN + 3LiNH_2 + KNH_2 + 8NaNH_2 \quad (6)$$

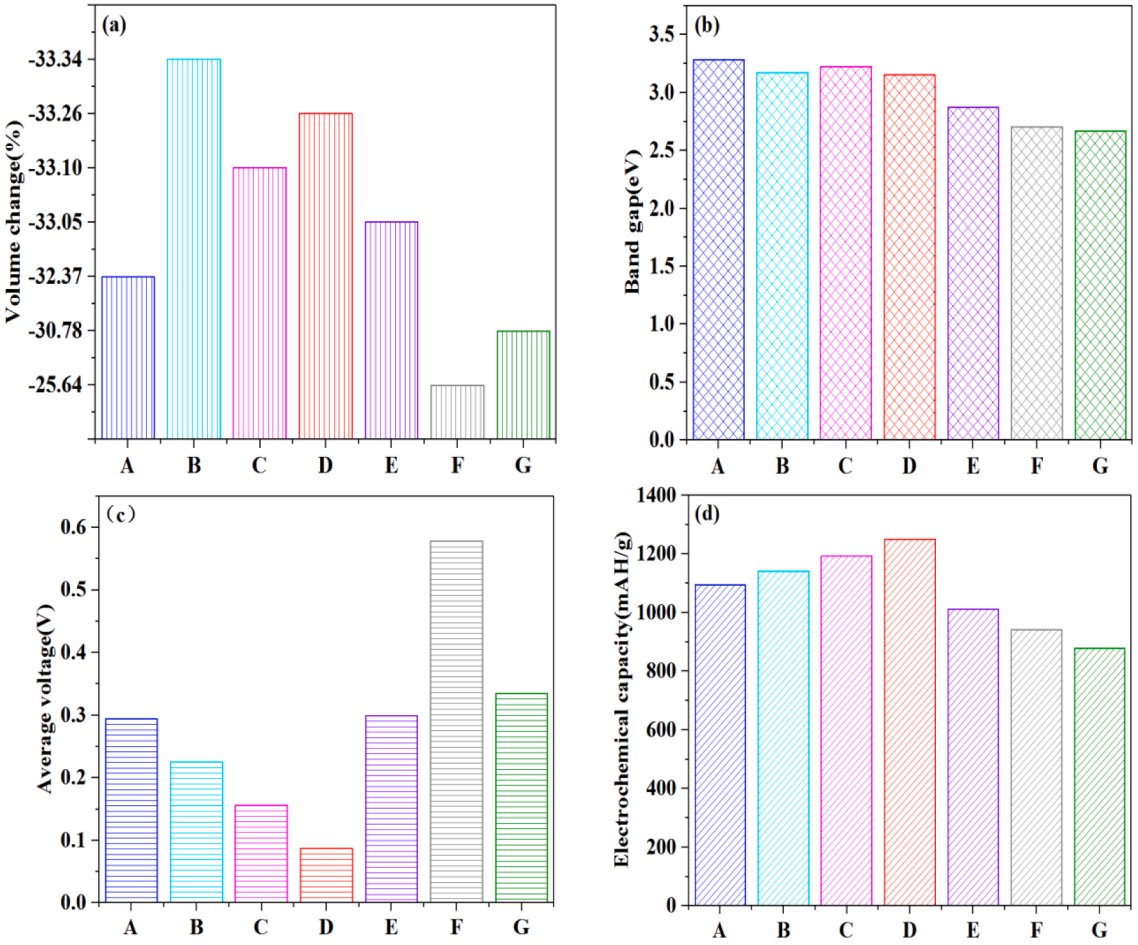

Fig. 3. Comparison of sodium-storage properties of $Li_4Al_4(N_4H_8)_4$ and its derivative materials: (a) volume change; (b) band gap; (c) average voltage versus Na^+/Na^0; (d) electrochemical specific capacity for sodium-storage. A: $Li_4Al_4(N_4H_8)_4$, B: $Li_4Al_3B(N_4H_8)_4$, C: $Li_4Al_2B_2(N_4H_8)_4$, D: $Li_4AlB_3(N_4H_8)_4$, E: $Li_3KAl_4(N_4H_8)_4$, F: $Li_2K_2Al_4(N_4H_8)_4$, G: $LiK_3Al_4(N_4H_8)_4$.

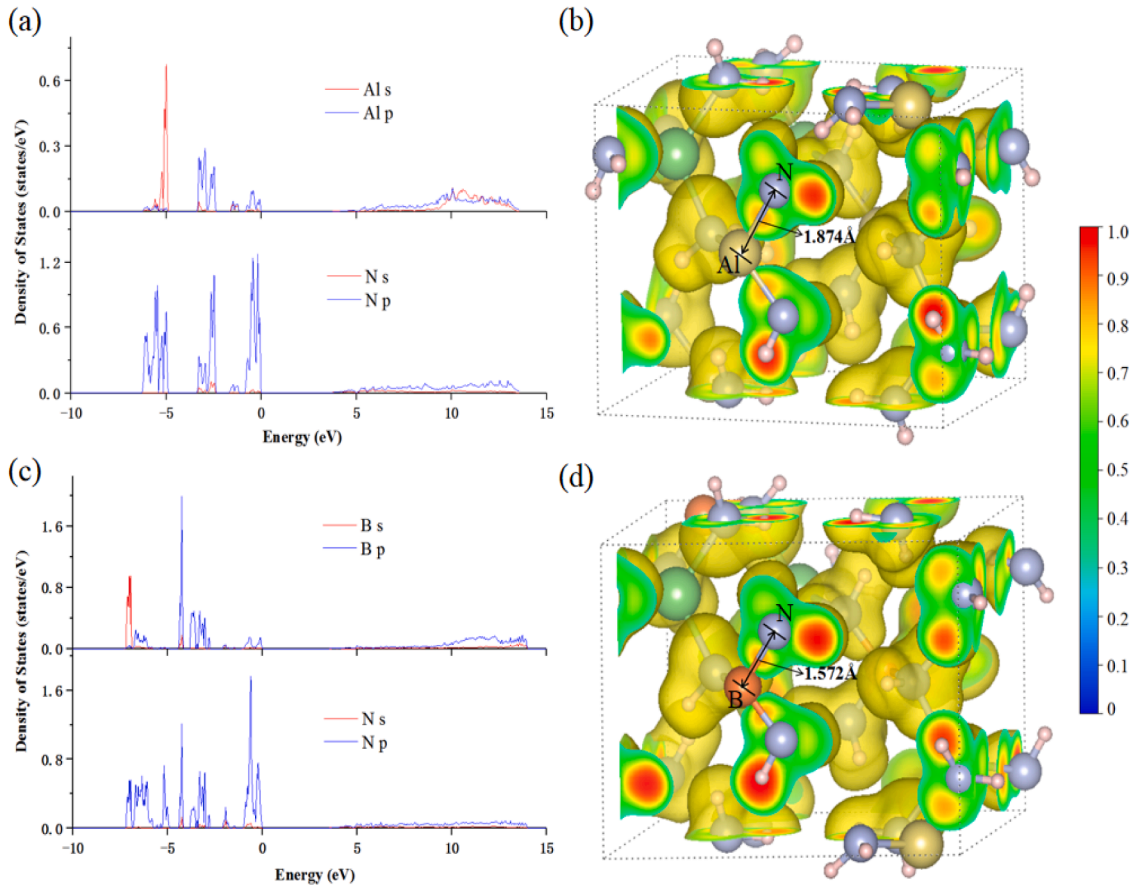

Fig. 4. The calculated partial density of states and electron localization function for $Li_4Al_4(N_4H_8)_4$ and $Li_4AlB_3(N_4H_8)_4$. (a) The partial DOS of the Al atom and N atom of $Li_4Al_4(N_4H_8)_4$; (b) the ELF of $Li_4Al_4(N_4H_8)_4$; (c) the partial DOS of the B atom and N atom of $Li_4AlB_3(N_4H_8)_4$; (d) the ELF of $Li_4AlB_3(N_4H_8)_4$. Al is shown in yellow sphere, N is in light blue and B is in orange. The Fermi level is set at zero. (For interpretation of the references to color in this figure legend, the reader is referred to the web version of this article.)

$$Li_2K_2Al_4(N_4H_8)_4 + 16Na^+ + 16e^- = 8NaH + 4AlN + 2LiNH_2 + 2KNH_2 + 8NaNH_2 \quad (7)$$

$$LiK_3Al_4(N_4H_8)_4 + 16Na^+ + 16e^- = 8NaH + 4AlN + LiNH_2 + 3KNH_2 + 8NaNH_2 \quad (8)$$

$$V \approx -\Delta G/F \quad (9)$$

$$\text{the specific capacity} = F{\cdot}n/3600M \quad (10)$$

To further analyze the electronic structures of $Li_4Al_4(N_4H_8)_4$ and $Li_4AlB_3(N_4H_8)_4$, the partial electronic density of states of the two materials are described in Fig. 4. As shown in Fig. 4(a), the p-state of Al and the p-state of N have overlapping in the vicinity of Fermi level. And in Fig. 4(c), the p-state of B and the p-state of N have overlapping around the Fermi level, indicating that B and N are chemically bonded. The electron localization functions of two materials are described in Fig. 4(b) and (d), respectively. The ELF value between Al and N atoms is close to 1, indicating that there is a distinct covalent bond between Al and N atoms. The ELF value between B and N atoms is also close to 1 in $Li_4AlB_3(N_4H_8)_4$. The charge between B-N bonds is more dense than that between Al-N bonds and the local bond length decreases to $d_{B\text{-}N} = 1.572$ Å from the pristine $d_{Al\text{-}N} = 1.874$ Å. In terms of their atomic structures, both B atoms and Al atoms have four coordination numbers and each atom forms a tetrahedral structure with four surrounding NH_2^- groups. The geometrically optimized lattice parameters of $Li_4AlB_3(N_4H_8)_4$ are: a = 9.250 Å, b = 7.297 Å, c = 7.288 Å and α = 90°, β = 91.90°, γ = 89.33° with a triclinic structure (space group of P1).

Table 2
Comparison of energy, unit-cell volume and charge state of Na when one Na-ion migrates to different sites of $Li_4Al_4(N_4H_8)_4$.

The migration sites	Energy (eV)	Volume (Å^3)	Charge state (e$^-$)
Li site	−295.314	579.170	+0.801
Al site	−295.338	592.494	+0.799
Interstitial site	−295.247	599.794	+0.792

Table 3
Comparison of energy, unit-cell volume and charge state of Na when one Na-ion migrates to different sites of $Li_4AlB_3(N_4H_8)_4$.

The migration sites	Energy (eV)	Volume (Å^3)	Charge state (e$^-$)
Li site	−302.691	561.122	+0.788
Al site	−302.650	554.581	+0.783
Interstitial site	−302.604	554.971	+0.797

The diffusion behavior of sodium ions in the electrode material is crucial for the kinetic performance during charging and discharging, thus it is indispensable to investigate the diffusion property of sodium-ions in electrode materials. Firstly, we considered a sodium ion in various sites of $Li_4Al_4(N_4H_8)_4$ lattice as well as $Li_4AlB_3(N_4H_8)_4$ and further calculated the thermodynamically most stable site to accommodate the sodium ion. The calculated results are given in Tables 2 and 3. The results suggest that the Na-ion tends to move to the Al-site in $Li_4Al_4(N_4H_8)_4$ lattice. While the Li-site is the most appropriate site to

Table 4
The diffusion coefficient of Na-ion in $Li_4Al_4(N_4H_8)_4$ and $Li_4AlB_3(N_4H_8)_4$ at 300 K and 400 K.

$Li_4Al_4(N_4H_8)_4$ at 300 K	$Li_4Al_4(N_4H_8)_4$ at 400 K	$Li_4AlB_3(N_4H_8)_4$ at 300 K	$Li_4AlB_3(N_4H_8)_4$ at 400 K
9.167×10^{-10} $m^2 s^{-1}$	1.500×10^{-9} m^2 s^{-1}	3.250×10^{-9} m^2 s^{-1}	3.667×10^{-9} m^2 s^{-1}

which the Na-ion tends to move in $Li_4AlB_3(N_4H_8)_4$. With respect to the charge circumstance inside the materials, the Bader charge analysis has been done to unveil the charge states of each atom in two materials (the full information can be found in Supplementary materials). Na has the charge state of $+0.799$ e^- when it migrates to the Al site in $Li_4Al_4(N_4H_8)_4$ and has the charge state of $+0.788$ e^- when it migrates to the Li site of $Li_4AlB_3(N_4H_8)_4$.Table 4.

After determining the most stable initial site(s), the *ab initio* molecular dynamics (AIMD) calculations have been conducted to analyze the diffusion coefficient of the Na-ion in $Li_4Al_4(N_4H_8)_4$ as well as $Li_4AlB_3(N_4H_8)_4$. The mean squared displacement (MSD) both at 300 K (room temperature) and at 400 K is calculated as described in Fig. 5. It is found that the Na-ion in the $Li_4AlB_3(N_4H_8)_4$ electrode diffuses faster than in $Li_4Al_4(N_4H_8)_4$ whether at 300 K or at 400 K.

The quantitative diffusion coefficients of Na-ion in both $Li_4Al_4(N_4H_8)_4$ and $Li_4AlB_3(N_4H_8)_4$ at 300 K and 400 K were further calculated through the Einstein equation:

$$\text{Diffusion coefficient D} = MSD/6N{\cdot}t \tag{11}$$

where N means the number of ions in the calculation model. The diffusion coefficient value of Na-ion in $Li_4AlB_3(N_4H_8)_4$ electrode is obviously increased to 3.250×10^{-9} $m^2 s^{-1}$. The results indicate that the modification with B element is very beneficial to the diffusion and migration of Na-ion, thereby greatly improving the electrochemical performance of pristine hydride for SIBs.

The diffusion route and energy barriers of Na-ion in $Li_4Al_4(N_4H_8)_4$ and $Li_4AlB_3(N_4H_8)_4$ have also been explored as shown in Figs. 6 and 7. We explored the diffusion of Na-ion from the middle of two Al atoms to the middle of two Li atoms in $Li_4Al_4(N_4H_8)_4$ and from the middle of two B atoms to the middle of two Li atoms in $Li_4AlB_3(N_4H_8)_4$. When the Na-ion diffuses in $Li_4Al_4(N_4H_8)_4$, the energy barrier is calculated to be 0.45 eV. Interestingly, the Na-ion only needs to surmount a small energy barrier of 0.31 eV in $Li_4AlB_3(N_4H_8)_4$, suggesting that the Na-ion is extremely easy to diffuse in $Li_4AlB_3(N_4H_8)_4$. In addition, compared with $Li_4Al_4(N_4H_8)_4$, the energy of the final state in the whole diffusion process is lower than that of the initial state in $Li_4AlB_3(N_4H_8)_4$, indicating that the diffusion process tends to more stable. These results suggest that the doping by B element will be highly beneficial to increase the potential

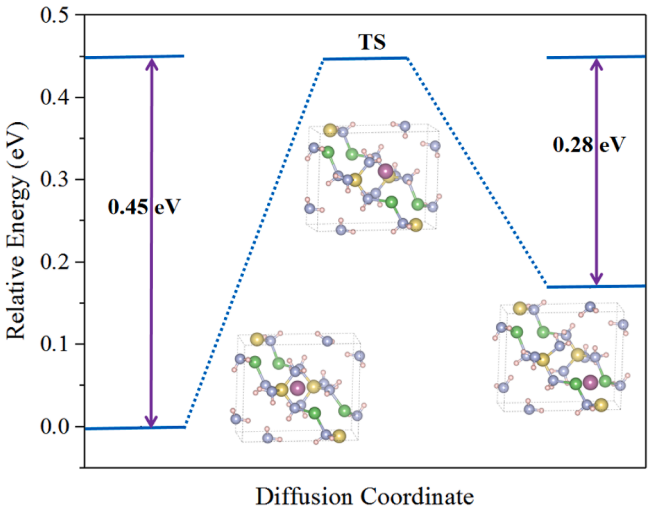

Fig. 6. Diffusion diagram of Na-ion (in purple color) in $Li_4Al_4(N_4H_8)_4$. TS refers to the transition state. (For interpretation of the references to color in this figure legend, the reader is referred to the web version of this article.)

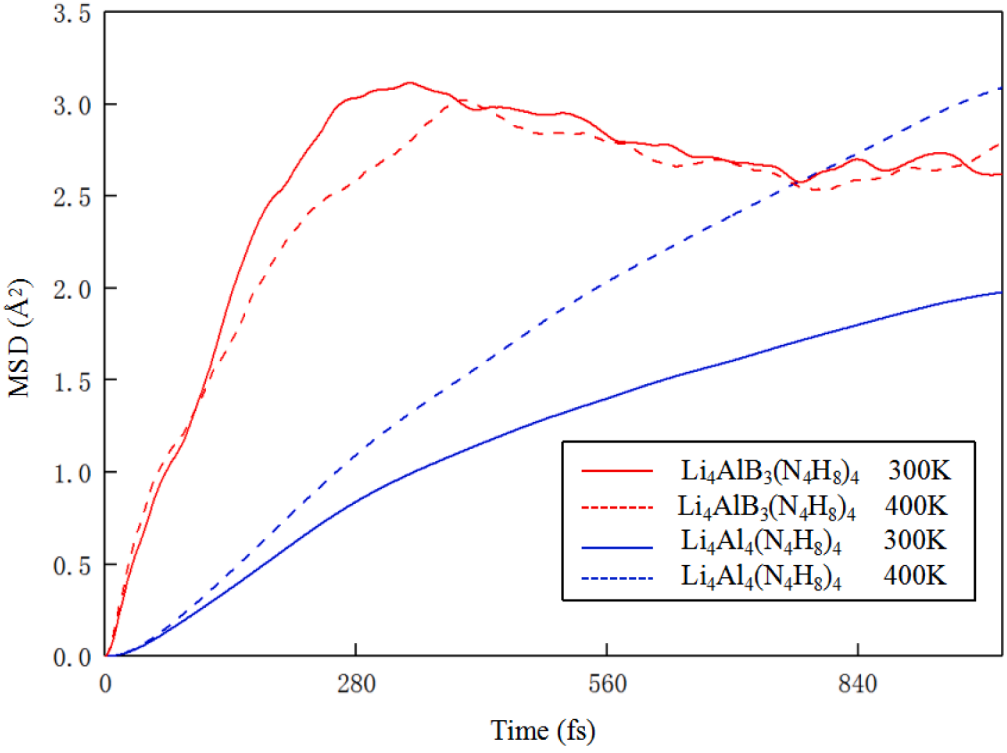

Fig. 5. The calculated mean squared displacement of Na-ion in $Li_4Al_4(N_4H_8)_4$ and $Li_4AlB_3(N_4H_8)_4$ through *ab initio* molecular dynamics (AIMD) technique at 300 K and 400 K.

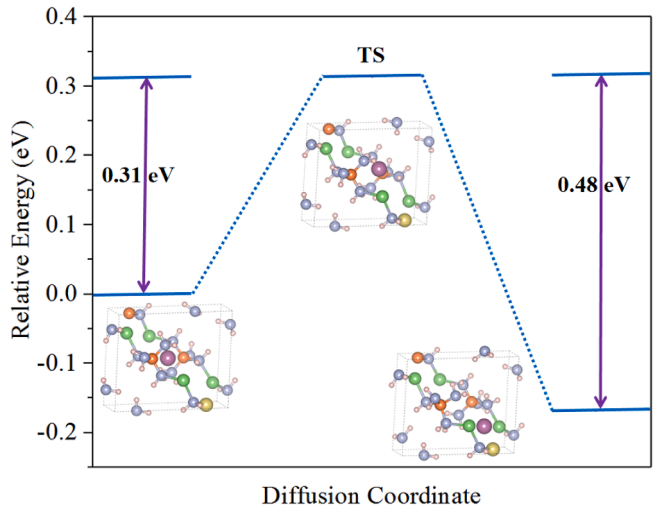

Fig. 7. Diffusion diagram of Na-ion (in purple color) in $Li_4AlB_3(N_4H_8)_4$. TS refers to the transition state. (For interpretation of the references to color in this figure legend, the reader is referred to the web version of this article.)

discharging/charging rates of the pristine electrode material.

Summary and outlook

In conclusion, the atomic and electronic structures as well as the electrochemical properties of light-metal based $LiAl(NH_2)_4$ and its modified compounds as conversion electrode materials for sodium-ion batteries have been detailedly investigated through DFT calculations. It is found that this material system (especially the derivative $Li_4AlB_3(N_4H_8)_4$ compound) has proper potential for conversion-type electrode applications for sodium storage, which possesses a theoretical specific capacity of 1249.57 mAh g^{-1} and a low average voltage of 0.087 V. The diffusion of Na-ion can be evidently enhanced in $Li_4AlB_3(N_4H_8)_4$ compared with the pristine $Li_4Al_4(N_4H_8)_4$ whether at 300 K (9.167×10^{-10} m^2 s^{-1} to 3.250×10^{-9} m^2 s^{-1}) or at 400 K (1.500×10^{-9} m^2 s^{-1} to 3.667×10^{-9} m^2 s^{-1}), which implies the potential rate capability of electrode materials at room temperature as well as high temperature when $Li_4Al_4(N_4H_8)_4$ is modified by the boron element. Besides, the diffusion coefficients of Na-ion in $Li_4Al_4(N_4H_8)_4$ and $Li_4AlB_3(N_4H_8)_4$ have also been unveiled through *ab initio* molecular dynamics (AIMD). The lower kinetic barrier of 0.31 eV in $Li_4AlB_3(N_4H_8)_4$ is very favorable for the migration of Na-ion. This quantum-mechanical based theoretical research will provide important clues for the new application of light-metal hydrides as conversion electrode materials in Na-ion batteries.

CRediT authorship contribution statement

Yingying Ren: Methodology, Writing - original draft. **Xiaohan Ren:** Data curation. **Rajeev Ahuja:** Writing - review & editing. **Zhao Qian:** Conceptualization, Methodology, Writing - review & editing, Project administration, Funding acquisition, Conceptualization, Methodology, Writing - review & editing, Project administration, Funding acquisition.

Declaration of Competing Interest

The authors declare that they have no known competing financial interests or personal relationships that could have appeared to influence the work reported in this paper.

Acknowledgements

This research was funded by the Natural Science Foundation of China (51801113), the Natural Science Foundation of Shandong Province (ZR2018MEM001, ZR2019BEE010), the Young Scholars Program of Shandong University (YSPSDU) and the Education Program of Shandong University (2020Y299). The HPC Cloud Platform of Shandong University is also acknowledged.

Appendix A. Supplementary data

Supplementary data to this article can be found online at https://doi.org/10.1016/j.rinp.2020.103408.

References

[1] Zhao C-L, Liu L, Qi X-G, Lu Y-X. Solid-state sodium batteries. Adv Energy Mater 2018;8:1703012.
[2] Cyrus W, Paul A, Venkat S. Resource constraints on the battery energy storage potential for grid and transportation applications. J Power Sources 2011;196:1593–8.
[3] Tarascon J-M. Key challenges in future Li-battery research. Phys Eng Sci 2010;368:3227–41.
[4] Cheng F-Y, Liang J, Tao Z-L, Chen J. Functional materials for rechargeable batteries. Adv Mater 2011;23:1695–715.
[5] Mortazavi M, Deng J-K, Shenoy V-B, Medhekar N-V. Elastic softening of alloy negative electrodes for Na-ion batteries. J Power Sources 2013;225:207–14.
[6] Grey C-P, Tarascon J-M. Sustainability and in situ monitoring in battery development. Nat Mater 2017;16:45–56.
[7] Lu X-C, Xia G-G, Lemmon J-P, Yang Z-G. Advanced materials for sodium-beta alumina batteries: status, challenges and perspectives. J Power Sources 2010;195:2431–42.
[8] Uebou Y, Okada S, Yamaki J. Electrochemical insertion of lithium and sodium into $(MoO_2)_2P_2O_7$. J Power Sources 2003;115:119–24.
[9] Wang L-C, Światowska J, Dai S. Promises and challenges of alloy-type and conversion-type anode materials for sodium–ion batteries. Mater Today Energy 2019;11:46–60.
[10] Oumellal Y, Rougier A, Nazri G-A, Tarascon J-M, Aymard L. Metal hydrides for lithium-ion batteries. Nat Mater 2008;7:916–21.
[11] Sartori S, Cuevas F, Latroche M. Metal hydrides used as negative electrode materials for Li-ion batteries. Appl Phys A 2016;122:122–35.
[12] El Kharbachi A, Zavorotynska O, Latroche M, Cuevas F, Yartys V, Fichtner M. Exploits, advances and challenges benefiting beyond Li-ion battery technologies. J Alloy Compd 2020;817:153261.
[13] El Kharbachi A, Andersen H-F, Yoshida K, Vajeeston P, Kim S, Sorby M, et al. Lithium ionic conduction in composites of $Li(BH_4)_{0.75}I_{0.25}$ and amorphous $0.75Li_2S{\cdot}0.25P_2S_5$ for battery applications. Electrochim Acta 2018;278:332–9.
[14] El Kharbachi A, Sørby M, Vullum P-E, Mæhlen J-P. Morphology effects in MgH_2 anode for lithium ion batteries. Int J Hydrogen Energy 2017;42:22551–6.
[15] Latroche M, Blanchard D, Cuevas F, El Kharbachi A. Full-cell hydride-based solid-state Li batteries for energy storage. Int J Hydrogen Energy 2019;44:7875–87.
[16] Brutti S, Meggiolaro D, Paolone A, Reale P. Magnesium hydride as negative electrode active material in lithium cells: a review. Mater Today Energy 2017;3:53–9.
[17] Møller K-T, Sheppard D, Ravnsbæk D-B, Buckley C-E, Akiba E, Li H-W, et al. Complex metal hydrides for hydrogen, thermal and electrochemical energy storage. Energies 2017;10:1645.
[18] Qian Z, Zhang H-N, Ren Y-Y, Ahuja R. Ab initio screening of doped $Mg(AlH_4)_2$ systems for conversion-type lithium storage. Materials 2019;12:2599.
[19] Tirado J-L. Inorganic materials for the negative electrode of lithium-ion batteries: state-of-the-art and future prospects. Mater Sci Eng R 2003;40:103–36.
[20] Obrovac M-N, Christensen L, Dahn J-R. Alloy design for lithium-ion battery anodes. J Electrochem Soc 2007;154:A849–55.
[21] Qian Z, Guo W-M, Jiang G-Z, Ahuja R, Liu X-F. Revisiting Mg–Mg_2Ni system from electronic perspective. Metals 2017;7:489.
[22] Park Y, Shin D, Woo S-H, Choi N-S. Sodium terephthalate as an organic anode material for sodium ion batteries. Adv Mater 2012;24:3562–7.
[23] Choi S-H, Kang Y-C. Synergetic compositional and morphological effects for improved Na^+ storage properties of Ni3Co6S8-reduced graphene oxide composite powders. Nanoscale 2015;7:6230–7.
[24] Chen P, Xiong Z-T, Luo J-Z. Interaction of hydrogen with metal nitrides and imides. Nature 2002;420:302–4.
[25] Hu J-J, Xiong Z-T, Wu G-T, Chen P. Hydrogen releasing reaction between Mg $(NH_2)_2$ and CaH_2. J Power Sources 2006;159:116–9.
[26] Zhang Z-Y, Zhang H-Z, Zhao H, Yu Z-S, He L, Li J. Prediction of the electronic structures, thermodynamic and mechanical properties in manganese doped magnesium-based alloys and their saturated hydrides based on density functional theory. J Power Sources 2015;280:147–54.
[27] Oelerich W, Klassen T, Bormann R. Metal oxides as catalysts for improved hydrogen sorption in nanocrystalline Mg-based materials. J Alloy Compd 2001;315:237–42.
[28] Hino S, Grove H, Ichikawa T. Metal aluminum amides for hydrogen storage – crystal structure studies. Int J Hydrogen Energy 2015;40:16938–47.

[29] Ayad M, Belkharroubi F, Boufadi F-Z, Khorsi M, Zoubir M-K, Ameri M, et al. First-principles calculations to investigate magnetic and thermodynamic properties of new multifunctional full-Heusler alloy Co_2TaGa. Indian J Phys 2020;94:767–77.
[30] Bekhti-Siad A, Bettine K, Rai D-P, Al-Douri Y, Wang X-T, Khenata R, et al. Electronic, optical and thermoelectric investigations of Zintl phase AE_3AlAs_3 (AE = Sr, Ba): First-principles calculations. Chin J Phys 2018;56:870–9.
[31] Benkaddour Y, Abdelaoui A, Yakoubi A, Khachai H, Al-Douri Y, Bin Omran S, et al. First-principle calculations of structural, elastic, and electronic properties of intermetallic rare earth R_2Ni_2Pb (R = Ho, Lu, and Sm) compounds. J Supercond Nov Magn 2018;31:395–403.
[32] Eymery J-B, Truflandier L, Charpentier T, Chotard J-N, Tarascon J-M, Janot R. Studies of covalent amides for hydrogen storage systems: structures and bonding of the $MAl(NH_2)_4$ phases with M=Li, Na and K. J Alloy Compd 2010;503:194–203.
[33] Qian Z, Jiang X, Maark T-A, Deshpande M-D, Bououdina M. Screening study of light-metal and transition-metal-doped NiTiH hydrides as Li-ion battery anode materials. Solid State Ionics 2014;258:88–91.
[34] Qian Z, De Sarkar A, Adit Maark T, Jiang X, Deshpande M-D, Bououdina M. Pure and Li-doped NiTiH: Potential anode materials for Li-ion rechargeable batteries. Appl Phys Lett 2013;103:033902.
[35] Jiang G-Z, Qian Z, Bououdina M, Ahuja R, Liu X-F. Exploring pristine and Li-doped Mg_2NiH_4 compounds with potential lithium-storage properties: ab initio insight. J Alloy Compd 2018;746:140–6.
[36] Kirklin S, Meredig B, Wolverton C. High-throughput computational screening of new Li-ion battery anode materials. Adv Eng Mater 2013;3:252–62.
[37] Bai X, Zhang B, Qian Z. Effective enhancement in rate capability and cyclability of $Li_4Ti_5O_{12}$ enabled by coating lithium magnesium silicate. Electrochim Acta 2019;295:891–9.
[38] Ouyang T-H, Qian Z, Hao X-P, Ahuja R. Effect of defects on adsorption characteristics of AlN monolayer towards SO_2 and NO_2: ab initio exposure. Appl Surf Sci 2018;462:615–22.
[39] Ouyang T-H, Qian Z, Ahuja R, Liu X-F. First-principles investigation of CO adsorption on pristine, C-doped and N-vacancy defected hexagonal AlN nanosheets. Appl Surf Sci 2018;439:196–201.
[40] Chen J-H, He X-J, Sa B-S, Zhou J. III–VI van der Waals heterostructures for sustainable energy related applications. Nanoscale 2019;11:6431–44.
[41] Lu Z-S, Pang Y-D, Li S. Phosphorene: a promising metal free cathode material for proton exchange membrane fuel cell. Appl Surf Sci 2019;479:590–4.
[42] Lu Z-S, Li S, Yang Z-X. The mechanism of oxygen activation on single Pt-atom doped SnO_2(110) surface. J Mater Sci 2016;51:10400–7.
[43] Al-Douri Y, Ameri M, Bouhemadou A, Batoo K-M. First-principles calculations to investigate the refractive index and optical dielectric constant of Na_3SbX_4 (X = S, Se) ternary chalcogenides. Phys Status Solidi B 2019;256:1900131–4.
[44] Benkaboua M-H, Harmela M, Haddoua M, Yakoubia A, Bakia N, Ahmedb R, et al. Structural, electronic, optical and thermodynamic investigations of $NaXF_3$ (X = Ca and Sr): first-principles calculations. Chin J Phys 2018;56:131–44.
[45] Bidai K, Ameri M, Amel S, Ameri I, Al-Douri Y, Varshney D, et al. First-principles calculations of pressure and temperature dependence of thermodynamic properties of anti-perovskite $BiNBa_3$ compound. Chin J Phys 2017;55:2144–55.
[46] Blanc X, Cancès E, Dupuy M-S. Variational projector augmented-wave method. Cr Math 2017;355:665–70.
[47] Lu Z-S, Li S, Yang Z-X. First principles study on the interfacial properties of NM/graphdiyne (NM = Pd, Pt, Rh and Ir): the implications for NM growing. Appl Surf Sci 2016;360:1–7.
[48] Lu Z-S, Yang M-X, Yang Z-X. CO oxidation on Mn-N4 porphyrin-like carbon nanotube: a DFT-D study Variational projector augmented-wave method. Appl Surf Sci 2017;426:1232–40.
[49] Shi S-Q, Ouyang C-Y, Lei M-S, Tang W-H. Effect of Mg-doping on the structural and electronic properties of $LiCoO_2$: a first-principles investigation. J Power Sources 2007;171:908–12.
[50] Rangel T, Caliste D, Genovese L, Torrent M. A wavelet-based projector augmented-wave (PAW) method: reaching frozen-core all-electron precision with a systematic, adaptive and localized wavelet basis set. Comput Phys Commun 2016;208:1–8.
[51] Kresse G, Furthmüller J. Efficiency of ab-initio total energy calculations for metals and semiconductors using a plane-wave basis set. Comput Mater Sci 1996;6:15–50.
[52] Perdew JP, Burke K, Ernzerhof M. Generalized gradient approximation made simple. Phys Rev Lett 1996;77:3865–8.
[53] Henkelman G, Uberuaga B-P, Jonsson H. A climbing image nudged elastic band method for finding saddle points and minimum energy paths. J Chem Phys 2000;113:9901–4.
[54] Wang G, Fazlur Rahman A-K, Wang B. Ab initio calculations of ionic hydrocarbon compounds with heptacoordinate carbon. J Mol Model 2018;24:116.
[55] Eymery J-B, Truflandier L, Charpentier T, Chotard J-N, Tarascon J-M, Janot R. A Studies of covalent amides for hydrogen storage systems: structures and bonding of the MAl(NH2)4 phases with M = Li, Na and K. J Alloy Compd 2010;503:194–203.
[56] Hino S, Grove H, Ichikawa T, Kojima Y, Sørby M-H, Hauback B-C. Metal aluminum amides for hydrogen storage-Crystal structure studies. Int J Hydrogen Energy 2015;40:16938–47.
[57] Ikeda K, Otomo T, Tsubota M, Suzuya K. Local structural analysis on decomposition process of $LiAl(ND_2)_4$. Mater Trans 2014;55:1129–33.
[58] Cui X-Y, Medvedeva J-E, Delley B, Newman N, Stampfl C. Role of embedded clustering in dilute magnetic semiconductors: Cr doped GaN. Phys Rev Lett 2005;95:256404.
[59] Ceder G, Aydinol M-K, Kohan A-F. Application of first-principles calculations to the design of rechargeable Li-batteries. Comput Mater Sci 1997;8:161–9.